# A sensitivity analysis of a FAO-56 dual crop coefficient-based model under various field conditions

Pierre Laluet, Luis Olivera-Guerra, Vincent Rivalland, Vincent Simonneaux, Jordi Inglada, Joaquim Bellvert, Salah Er-Raki, Olivier Merlin

# Journal Pre-proof

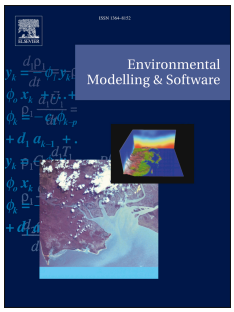


A sensitivity analysis of a FAO-56 dual crop coefficient-based model under various field conditions

Pierre Laluet, Luis Olivera-Guerra, Vincent Rivalland, Vincent Simonneaux, Jordi Inglada, Joaquim Bellvert, Salah Er-raki, Olivier Merlin

PII: S1364-8152(22)00308-5

DOI: https://doi.org/10.1016/j.envsoft.2022.105608

Reference: ENSO 105608

To appear in: *Environmental Modelling and Software*

Received Date: 1 July 2022

Revised Date: 9 December 2022

Accepted Date: 12 December 2022

Please cite this article as: Laluet, P., Olivera-Guerra, L., Rivalland, V., Simonneaux, V., Inglada, J., Bellvert, J., Er-raki, S., Merlin, O., A sensitivity analysis of a FAO-56 dual crop coefficient-based model under various field conditions, *Environmental Modelling and Software* (2023), doi: https://doi.org/10.1016/j.envsoft.2022.105608.

# A sensitivity analysis of a FAO-56 dual crop coefficient-based model under various field conditions

Pierre Laluet [a], Luis Olivera-Guerra [a], Vincent Rivalland [a], Vincent Simonneaux [a], Jordi Inglada [a], Joaquim Bellvert [b], Salah Er-raki [c,d], Olivier Merlin [a]

[a] Centre d'Etudes Spatiales de la Biosphère (CESBIO), Université de Toulouse, CNES, CNRS, IRD, UPS, Toulouse, France

[b] Efficient Use of Water in Agriculture Program, Institute of AgriFood, Research and Technology (IRTA), Parc Científic I Tecnològic Agroalimentari de Gardeny (PCiTAL), Fruitcentre, 25003 Lleida, Spain

[c] ProcEDE, AgroBiotech Center, Département de Physique Appliquée, Faculté des Sciences et Techniques, Université Cadi Ayyad, Marrakech, Morocco

[d] Mohammed VI Polytechnic University (UM6P), Center for Remote Sensing Applications (CRSA), Morocco

Abstract

FAO-56 dual crop coefficient (FAO-2Kc) based model are increasingly applied at large scale for agricultural water monitoring, requiring field-scale data over the spatial extent of interest. Given the lack of in-situ measurements, satellite products can be used to estimate indirectly the parameters through calibration. However, a lack of knowledge about model sensitivity can lead to suboptimal use of satellite data. This study aims to analyze the sensitivity of SAMIR, a FAO-2Kc-based model using satellite data. The Sobol method was applied for evapotranspiration (ET) and deep percolation (DP) simulations on 37 contrasted agricultural seasons. Results indicate that SAMIR's sensitivity mainly depends on the modeled water stress. We proposed a proxy for the model sensitivity which can determine 84% (73%) of the ET (DP) among the agricultural seasons. An interaction analysis allowed reducing the calibration problem to the adjustment of only two parameters (a_Kcb and Zr_max), accounting for most of the sensitivity.

Keywords

FAO-56 model; Sobol sensitivity analysis; Evapotranspiration; Deep percolation; Remote sensing; Calibration

## 1. Introduction

Irrigation is the most water-intensive anthropogenic activity in the world. The resources available for it are already under pressure in some regions and will be even more so in the future (FAO, 2011). To face these challenges, crop water balance models are widely used with the aim of optimizing agricultural water use (Pereira et al., 2020; Constantin et al., 2015). Such models seek to estimate the crop water consumption and irrigation needs by simulating all the terms of the crop water balance, including evapotranspiration (ET, corresponding to crop consumption) and deep percolation (DP, being an indicator of water loss for crops).

The dual crop coefficient version (FAO-2Kc) of the FAO-56 method (Allen et al., 1998) is based on the estimation of actual ET coupled to a soil water balance. The FAO-2Kc method has been widely used in both operational and academic contexts for its efficiency and parsimony (more than 30,000 citations of the FAO-56 method (Pereira et al., 2021)). From the same basic FAO-2Kc formulation, many models have been developed with their own specificities, like the representation of additional processes (e.g., runoff, capillary rise), a more detailed description of specific processes (e.g. DP, root development, soil evaporation), or the use of satellite data (Helman et al. 2019; Olivera-Guerra et al., 2018; Han et al., 2018; Bellvert et al. 2018; Campos et al., 2017; Yang et al., 2012; Rosa et al, 2012a, b; Raes et al., 2009; Lollato et al., 2016; Sheikh et al., 2009). In the same vein, the SAMIR (Satellite Monitoring for IRrigation, Simonneaux et al., 2009) model, which is used in this work, is a FAO-2Kc-based model integrating remotely sensed Normalized Difference Vegetation Index (NDVI) to constrain the vegetative growth. It includes 12 parameters related to soil and crop type characteristics.

The FAO-2Kc method can simulate ET and DP at the plot or at the pixel scale, which when aggregated can provide simulations of both fluxes at integrated spatial scales (irrigation district or catchment) using mapped input data (Kharrou et al., 2021; Garrido-Rubio et al., 2020; Bretreger et al., 2019). The FAO-2Kc requires i) maps of meteorological forcings, ii) maps of irrigation forcings, iii) maps of crop type to derive crop parameters, and iv) maps of soil texture to derive soil parameters. Those maps are becoming increasingly available and accurate thanks to the development of i) reanalysis meteorological data sets at enhanced resolutions (e.g. ERA5 (Hersbach et al., 2020), SAFRAN (Vidal et al., 2010)), ii) maps of actual irrigation type, volume, and timing derived from satellite observations (Massari et al.,

2021), iii) crop type maps whether they come from field observations or classifications based on satellite observations (Foerster et al., 2012; Inglada et al., 2015), and iv) soil texture maps (e.g. SoilGrids (Hengl et al., 2017), GlobalSoilMap (Arrouays et al., 2017)). However, such data sets still have significant uncertainties due to intrinsic errors in the mapped data, and to additional errors associated with their conversion to directly usable input parameters (e.g., hydrodynamical soil properties are usually derived from soil texture maps) (Poggio et al., 2021, Folberth et al., 2016, Loosvelt et al., 2012). It is thus often necessary to calibrate the model input parameters using external data. Such a calibration strategy can be implemented at the field scale using in-situ measurements (Kharrou et al., 2021; Saadi et al., 2015; Paredes et al., 2014; Er-Raki et al., 2007; Zhang et al., 2013), or over extended areas using remotely sensed soil moisture or ET data (Amazirh et al., 2022; Ouaadi et al., 2021; Er-Raki et al., 2008).

To reduce uncertainties in spatially distributed model input parameters, many works have dealt with the assimilation of remotely sensed soil moisture (Brocca et al., 2014; Azimi et al., 2020; Zaussinger et al., 2019) and ET (Wu et al., 2015; Droogers et al., 2010) products. By minimizing sequentially and recursively the gap between simulations and observations, it is possible to indirectly retrieve optimal values of a set of input parameters or at least to reduce their a priori uncertainty. However, this approach may face difficulties in terms of practical implementation due to its extensive requirement in terms of computational resources. Calibrating an agro-hydrological model over large areas may indeed require a large number of simulations. This is especially true when models have a considerable number of input parameters (from a dozen (Simonneaux et al., 2009) to several dozen (Neitsch et al., 2011)) and when they are spatialized over several thousands of pixels or fields. In addition, the calibration of many parameters from limited observations raises the issue of equifinality. An equifinality occurs when several parameter sets lead to a result considered as optimal. This can be problematic because each of these parameter sets does not necessarily have any likelihood with the physical reality of the parameters—physical reality of which we can have prior knowledge (Beven et al., 2001, 2006).

A solution to the above concerns is to analyze the sensitivity of the studied model in order to identify and calibrate the parameters having the most influence on the outputs. Indeed, focusing only on the most sensitive parameters may significantly reduce the required computer resources, in addition to limiting the compensation issues between parameters.

Even though models based on the FAO-2Kc method are widely used, the study of their sensitivity to input parameters is not or almost not present in the scientific literature. Olivera-Guerra et al. (2020) analyzed the sensitivity of three soil parameters (soil moisture at field capacity, at wilting point, and the maximum roots depth (Zr_max)) of SAMIR using a local sensitivity analysis method, i.e., by varying independently each of the parameters and looking at their impact on an objective function. However, for a comprehensive analysis—and this is especially required when the number of analyzed parameters is larger—global sensitivity analysis methods are strongly recommended (Saltelli and Annoni, 2010; Song et al., 2015). Global sensitivity analysis methods can calculate the influence of input parameters over their entire range of variation and are appropriate for all types of models (non-linear and non-monotonic). The Sobol variance-based method (Sobol, 1993, 2001; Saltelli et al., 2008, 2010) is a popular global sensitivity analysis method that has been used in many recent articles because of its robustness and of its ability to analyze interactions between parameters (Nossent et al., 2011; Baroni and Tarantola, 2014; Tang et al., 2007; Zhang et al., 2013). The principle of the Sobol method is to decompose the total variance of a model's output and to look at how each uncertain parameter contributes to it, whether this contribution is caused only by a single parameter or by the interaction of two or more parameters.

In this context, the objective of this paper is to perform a Sobol sensitivity analysis of the FAO-2Kc-based SAMIR model, for both output fluxes ET and DP. To ensure the analysis results are representative of the field conditions where the FAO-2Kc method is generally implemented, ten fields and a total of 37 agricultural seasons were selected based on their contrasted meteorological, pedological, and agricultural characteristics.

The paper is organized as follows. The SAMIR model, data sets, and the Sobol method are first described (Section 2). Then the results of the Sobol sensitivity analysis are discussed for both ET and DP (Section 3), with the overall goal of identifying the most influential parameters depending on actual field conditions. Finally, the conclusions and perspectives are presented (Section 4).

## 2. Material and methods

The overall methodology to assess the sensitivity of the SAMIR model to its input parameters is presented in the flowchart of Figure 1. First, SAMIR is presented together with its 12 input

parameters (section 2.1). Then the input data composed of forcing (precipitation, irrigation, NDVI), crop type, and soil properties are described (section 2.2). The next three subsections describe the main steps of the sensitivity analysis approach that are: calculating the Sobol indices for each of the parameters and each target variable ET and DP (section 2.3), sampling the SAMIR parameters with normal distributions defined for each agricultural season (section 2.4), and running SAMIR on the generated samples and computing performance metrics (section 2.5). Finally, a proxy for the sensitivity of SAMIR ET and DP simulations is investigated from the variability of Sobol indices (section 2.6).

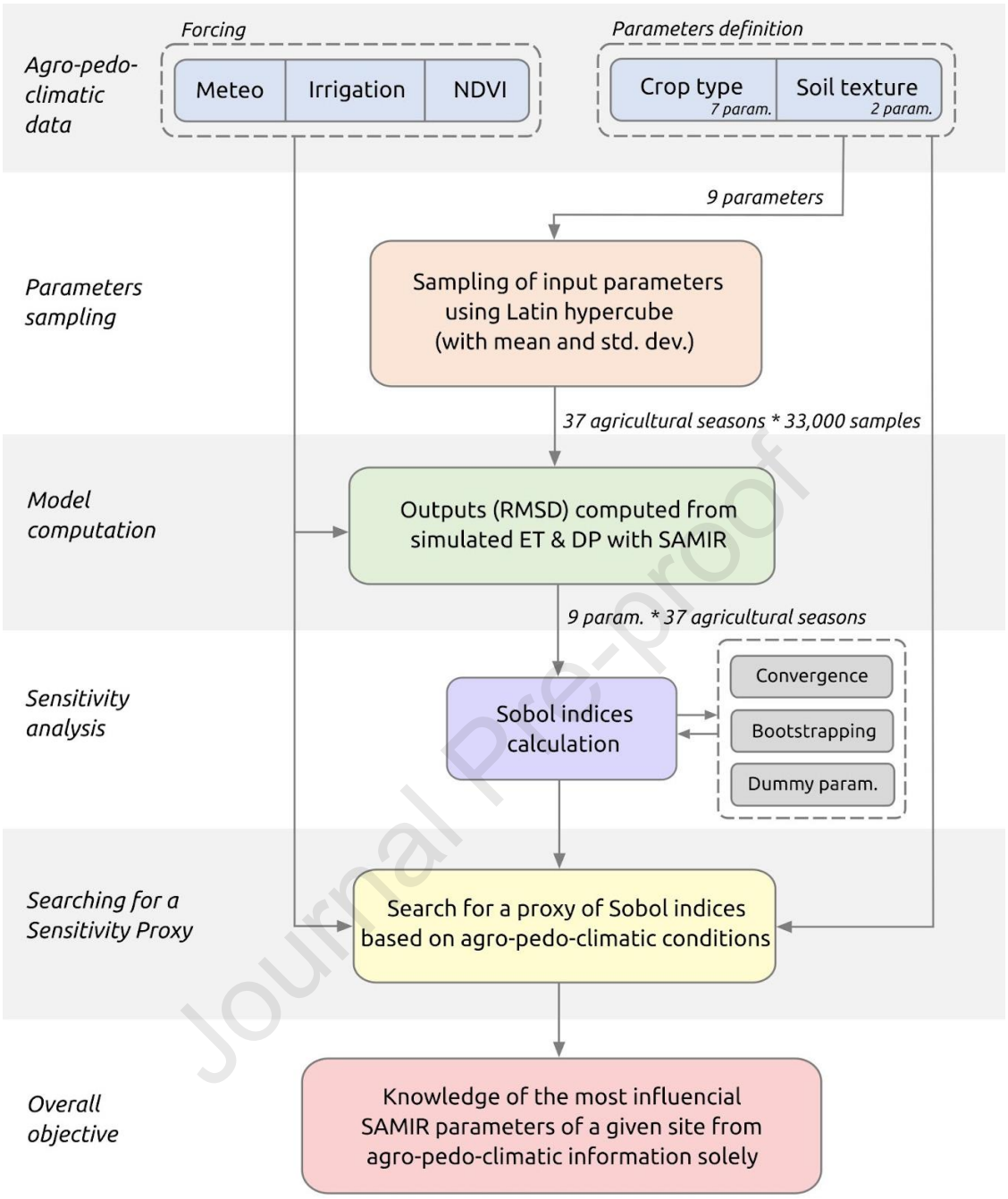


Figure 1: Flowchart of the methodology to assess the sensitivity of the SAMIR model to its input parameters.

## 2.1. Satellite Monitoring for IRrigation (SAMIR) model

The SAMIR (Simonneaux et al., 2009) model used in this study is based on the FAO-2Kc method. While a detailed description of the FAO-2Kc method is provided in Allen et al. (1998), only the main components are briefly reminded below as well as the main differences

between this method and the SAMIR model. For a more detailed overview of the SAMIR model, readers are encouraged to refer to Saadi et al. (2015).

The principle of the FAO-2Kc method is the calculation of crop water balance components for daily ET estimation, taking into account the plants and the soil water status. It uses i) meteorological forcing variables to calculate the reference ET (called ET0), ii) precipitation and irrigation amounts resulting in water available for ET or for soil reservoir recharge, iii) crop and soil parameters to compute soil reservoir properties as well as plant and soil resistance to water stress, and iv) the initial soil water content at the start date of model simulations. In addition to these variables and parameters, the SAMIR model incorporates remotely sensed NDVI time series to drive the development of the modeled vegetation.

The daily water balance equation simulated by SAMIR is:

$$P + I = ET + DP + \Delta SW \quad (1)$$

with P being the precipitation, I the irrigation, ET the actual evapotranspiration, ΔSW the variation of soil water content from the previous day, and DP the deep percolation being the water exceeding the maximum soil storage capacity.

The ET calculation is done by applying crop coefficients to ET0 as follow:

$$ET = ET0(Kcb \cdot Ks + Ke) \quad (2)$$

where ET0·Kcb·Ks is the water transpired by plants (T) and ET0·Ke is the soil evaporation (E). In equation (2), ET0 is calculated according to the FAO Penman-Monteith equation (Allen et al., 1998), Kcb is the basal crop coefficient following a linear relationship with NDVI, Ks is the water stress coefficient being a reduction factor of T, and Ke is the soil evaporative coefficient being related to vegetation fraction cover (Fc), surface soil moisture and soil properties. Similarly to Kcb, Fc follows a linear relationship with NDVI.

In addition to the use of NDVI time series, SAMIR incorporates two additional modifications from the classical FAO-2Kc method:

i) The Kr evaporation reduction coefficient, accounting for soil evaporation resistance as a function of surface soil moisture, is calculated with the method proposed by Merlin et al. (2016). This method, instead of using an a priori parameterization, uses a pedotransfer function based on clay and sand fractions ($f_{clay}$ and $f_{sand}$) which was derived and evaluated

over a variety of sites and soil textures (Merlin et al., 2016; Lehmann et al., 2018; Amazirh et al., 2021).

ii) The soil moisture values at field capacity and at wilting point are calculated using $f_{clay}$ and $f_{sand}$ from the pedotransfer function proposed by Román Dobarco et al. (2019).

SAMIR uses a total of 12 user-defined parameters: six parameters related to the plants phenological stage and T capabilities (that we named the PHENO parameters), five parameters related to soil reservoir properties and plant resistances to stress (that we named the STRESS parameters), and one parameter used to set the soil water content at the start date of model simulations. A detailed description of the parameters is provided in Table 1, with their definition and the processes in which they are involved.

| Parameter | Definition | Process involved | Type of parameter |
|---|---|---|---|
| a_Fc (-) | Linear relationship between Fc and NDVI (Fc=a_Fc·NDVI+b_Fc) | E/T partitioning, roots development | PHENO |
| b_Fc (-) | | | PHENO |
| a_Kcb (-) | Linear relationship between Kcb and NDVI (Kcb=a_Kcb·NDVI+b_Kcb) | Vegetation development, T demand | PHENO |
| b_Kcb (-) | | | PHENO |
| Zr_max (mm) | Maximum root depth | Root reservoir size, triggering of T reduction due to water stress | STRESS |
| p (-) | Stress threshold coefficient (plant resistance to water stress) | Triggering of T reduction due to water stress | STRESS |
| $f_{clay}$ (-) | Clay fraction in the soil column | Soil reservoir water holding capacity, triggering of T and E reduction due to water limitation | STRESS |
| $f_{sand}$ (-) | Sand fraction in the soil column | | STRESS |

| | | | |
|---|---|---|---|
| Ze (mm) | Surface soil layer depth | E | STRESS |
| Kcb_max (-) (not analyzed) | Maximum Kcb value | Maximum plant T demand | PHENO |
| Kc_max (-) (not analyzed) | Maximum value of Kcb+Ke | Maximum ET demand | PHENO |
| Init_hum (-) (not analyzed) | Soil water content at the first day of the model simulation | Crop water budget | - |

Table 1: List of the SAMIR parameters and physical processes in which they are involved.



2.2. Sites and data description

Data of 37 agricultural seasons from ten different crop fields around the world were used. They were obtained from national and international databases, or from specific intensive field campaigns. The agricultural seasons cover a wide variety of agro-pedo-climatic conditions that reflect the contexts of use of SAMIR, i.e., different crop types mainly located in dry areas where water-related agricultural issues are important, but also and to a lesser extent, in temperate areas where ET estimation may also be key for a good water management. The data set involves 13 crop types including summer and winter cereals, vegetables, and fruit trees; 10 soil textures ranging from clay to silty loam; 4 irrigation types (flood irrigation, sprinkler, drip irrigation, no irrigation); and 2 different climates (semi-arid and temperate). Table 2 reports the characteristics of each agricultural season.

The data used for running SAMIR are composed of i) meteorological variables obtained from local weather stations for precipitation and ET0 calculation (air temperature, wind speed, solar radiation, and relative air humidity), ii) irrigation dates and amounts obtained from water meters, iii) crop types, iv) soil texture ($f_{clay}$ and $f_{sand}$), and v) NDVI time series obtained from Sentinel-2A and 2B and Landsat 7 and 8. The Sentinel-2 constellation provides a 10-meter resolution pixel with a temporal resolution of 10 days from 2015 and 5 days since 2017, in clear sky conditions. Landsat 7 provides 30-meter resolution pixels with a 16-day

time resolution since 1999. Landsat 8 has the same characteristics but has been available since 2013, and its overpass is offset by 8 days with respect to Landsat 7.

It is important to note that for all agricultural seasons, the periods studied ranged from the beginning of the vegetation development to the end of the senescence period. Periods between successive agricultural seasons with bare soil or low evaporative demand were not considered herein because this study only assessed the sensitivity of ET and DP when the major part of crop's water consumption occurs.

| Agricultural season label | Country | Climate (P; ET0, in mm) | Irrigation type | $f_{clay}$ (-) | $f_{sand}$ (-) | Reference |
|---|---|---|---|---|---|---|
| AUR_Sunflower_07 | France | Temperate (640; 1020) | None | 0.32 | 0.20 | Béziat et al. (2009) |
| AUR_Wheat_06 | | | | | | |
| AUR_Wheat_08 | | | | | | |
| AUR_Wheat_10 | | | | | | |
| CAT_Apple_20 | Spain | Semi-arid (420; 1000) | Drip | 0.24 | 0.36 | Domínguez-Niño et al. (2019) |
| CAT_Apple_21 | | | | | | |
| CAT_Maize1_21 | Spain | | Sprinkler | 0.36 | 0.20 | This study |
| CAT_Maize2_21 | | | | 0.29 | 0.16 | |
| CAT_Wine_20 | Spain | | Drip | 0.55 | 0.10 | Bellvert et al. (2020) |
| CAT_Wine_21 | | | | | | |
| LAM_Maize_06 | France | Temperate (640; 1020) | Sprinkler | 0.54 | 0.12 | Béziat et al. (2009) |
| LAM_Maize_08 | | | | | | |
| LAM_Maize_10 | | | | | | |

| | | | | | | |
|---|---|---|---|---|---|---|
| LAM_Maize_12 | | | | | | |
| LAM_Maize_14 | | | | | | |
| LAM_Maize_19 | | | | | | |
| LAM_Wheat_07 | | | None | | | |
| LAM_Wheat_09 | | | | | | |
| LAM_Wheat_11 | | | | | | |
| BOUR_Wheat_16 | Morocco | Semi-arid (220; 1500) | None | 0.41 | 0.18 | Merlin et al. (2018) |
| BOUR_Wheat_17 | | | | | | |
| BOUR_Wheat_18 | | | | | | |
| CHI_Wheat_16 | Morocco | | Drip | 0.33 | 0.38 | Rafi et al. (2019) |
| MAR_Wheat1_02 | Morocco | | Flood | 0.47 | 0.19 | Er-Raki et al. (2007) |
| MAR_Wheat2_02 | | | | | | |
| MAR_Wheat3_02 | | | | | | |
| MAR_Wheat4_15 | | | | | | |
| MAR_Wheat5_15 | | | Drip | | | |
| MEX_Bean_08 | Mexico | Semi-arid (250; 2050) | Drip | 0.44 | 0.36 | Chirouze et al. (2014) |
| MEX_Chilli_08 | | | | | | |
| MEX_Chickpeas_08 | | | Flood | | | |
| MEX_Broccoli_08 | | | | | | |
| MEX_Potatoes_08 | | | | | | |

| | | | | | | |
|---|---|---|---|---|---|---|
| MEX_Sorghum_08 | | | | | | |
| MEX_Wheat1_08 | | | | | | |
| MEX_Wheat2_08 | | | | | | |
| TUN_Barley_12 | Tunisia | Semi-arid (270; 1310) | Flood | 0.33 | 0.33 | Saadi (2018) |
| TUN_Wheat1_12 | | | | | | |
| TUN_Wheat2_12 | | | None | | | |

Table 2: Agricultural seasons included in the sensitivity analysis and their main characteristics.



2.3. Sobol sensitivity analysis

2.3.1. Sobol indices

A general overview of the Sobol method is presented here, while more detailed descriptions can be found in Saltelli et al. (2008, 2010), or Khorashadi Zadeh et al. (2017).

Consider a model Y=f(X)=f($X_1$,…,$X_k$) with k parameters, where Y is the model output (e.g., a performance metric such as the root mean square difference), and X=($X_1$,…,$X_k$) the parameter set, which can be decomposed into $2^k$ terms representing different order of interaction between parameters:

$$f(X_1,\dots,X_k) = f_0 + \sum_{i=1}^{k} f_i(X_i) + \sum_{i=1}^{k}\sum_{j=i+1}^{k} f_{ij}(X_i,X_j) + \dots + f_{1,\dots,k}(X_1,\dots,X_k) \quad (3)$$

The total output variance of the model V(Y) can be decomposed into corresponding partial variances:

$$V(Y) = \sum_{i=1}^{k} V_i + \sum_{i=1}^{k-1}\sum_{j=i+1}^{k} V_{ij} + \dots + V_{1,\dots,k} \quad (4)$$

The first-order index Si, also called main effect, is the ratio between $V_i$ in equation (4) and the total output variance V(Y). Si can be written as follows:

$$S_i = \frac{V_i}{V(Y)} = \frac{V_{X_i}\left(E_{X_{\sim i}}[Y|X_i]\right)}{V(Y)} \quad (5)$$

The total index $ST_i$ represents the sum of $X_i$'s main effect with all its higher-order interactions up to order k. $V_{\sim i}$ is the variance resulting from the contribution of all parameters except $X_i$. It can be written as follows:

$$ST_i = 1 - \frac{V_{\sim i}}{V(Y)} = \frac{E_{\boldsymbol{X}_{\sim i}}\left[V_{X_i}(Y|X_{\sim i})\right]}{V(Y)} \quad (6)$$

STi index is the one we used in this study to evaluate the sensitivity of SAMIR parameters. Indeed, STi, unlike Si, integrates all the influence a parameter has on a model output, which is of interest to determine the most sensitive parameters. Si is used to calculate the interactions a parameter has with the others, by calculating the difference between STi and Si. If the sum of the Si is equal to 1, it means that the model is linear and that there is no interaction between the parameters. On the contrary, if the sum of the Si is smaller than 1, the model is non-linear. The lower the sum of the Si, the more the parameters of the model interact with each other.

The SAFE Toolbox (Pianosi et al., 2015) was used in this study in order to perform the Sobol indices calculation and generate the samples.

2.3.2. Convergence analysis

For each agricultural season, a convergence analysis of Si and STi was done in order to verify that the number of simulations is sufficient to ensure their stability. Results (not shown) indicated that N=n(k+2)=33,000 (with n=3,000 and k=9 parameters) is sufficient for all the 37 agricultural seasons.

2.3.3. Bootstrapping

In order to optimally take into account the uncertainties (related to the distribution of the model outputs) in the STi and Si values we used, a bootstrapping technique was applied (Efron and Tibshirani, 1994). This technique consists of randomly resampling the 33,000 model outputs 1,000 times and recalculating the Sobol indices for each resampled data set. Then, the average of Si and STi is derived from the 1,000 resamples and can be kept for the sensitivity analysis.

2.3.4. Dummy parameter

A dummy parameter, a parameter added to the analysis that we know has no influence on the model output, was introduced in this sensitivity analysis. For further explanation on the calculation of the dummy parameter, readers are encouraged to refer to Khorashadi Zadeh et al. (2017). The STi calculated for the dummy parameters were used herein as thresholds to identify sensitive parameters from insensitive parameters. They were also used to ease the readability of the STi values, by normalizing them for each agricultural season between the dummy parameter's STi and the sum of all parameters' STi. It is then called $STi_{norm}$ and is expressed as a percentage.

2.4. Parameters sampling

2.4.1. Latin hypercube sampling

Despite its popularity, the Sobol sensitivity analysis method can be challenging to implement due to its high computational cost. It requires a total of $N=n(k+2)$ samples, with n a baseline sample size that can vary between 1,000 to more than 10,000, and k the number of analyzed parameters. To optimize the sampling efficiency, the Latin hypercube sampling method (LHS) was used. LHS is a Monte Carlo-based method using a stratified sampling approach where the distribution of each parameter is divided into P ranges, each with a probability of occurrence of 1/P. Parameter values are randomly generated so that each range gets sampled only once. The same step is repeated for each of the k parameters to generate a matrix of size $P \cdot k$ with random sample combinations of the different parameters. The LHS method has been used in many studies, e.g., Campolongo et al. (2011), Saltelli and Annoni (2010), Zhang et al. (2013), Tang et al. (2007) and Song et al. (2015).

2.4.2. Parameters' mean and standard deviation

Nine parameters were sampled and analyzed out of the 12 included in SAMIR. Of these, three parameters were fixed: Kcb_max, Kc_max, and Init_hum (see Table 1). For Kcb_max and Kc_max, a previous analysis (not shown) performed on six contrasted agricultural

seasons indicated that their sensitivity is negligible. The main explanation lies in the way the Kcb-NDVI relationships are constructed (using minimum and maximum NDVI values from satellite observations), limiting the number of days when these parameters can influence ET. Regarding Init_hum, we considered it as a forcing data and set it to its median value (0.5), because soil moisture measurements at the beginning of agricultural seasons were not available for all sites.

The parameters analyzed were sampled according to a normal distribution using mean and standard deviation values. To make the link with the LHS method mentioned in section 2.4.1, the normal distributions obtained for each parameter were divided into P intervals of equal probability—intervals being then more or less narrow depending on the parameter's distribution. The mean values of the nine parameters were defined for each agricultural season from: i) field analyses for $f_{clay}$ and $f_{sand}$, ii) literature references for Zr_max, p, and Ze, and iii) satellite observations for NDVI-related parameters (a_Fc, b_Fc, a_Kcb, and b_Kcb). The standard deviation of crop-related parameters (Zr_max, p, a_Fc, b_Fc, a_Kcb, and b_Kcb) vary according to the crop type. It allows us to represent the uncertainty of a given parameter as a function of the mean value of this parameter, and therefore according to the crop type. For example, Zr_max of broccoli crops (having a mean Zr_max of 500 mm) has a smaller uncertainty—and therefore a smaller standard deviation—than Zr_max of maize crops having a mean value of 1050 mm. Since maize has been extensively investigated, the standard deviations of its parameters were chosen as a reference. Therefore, the ratios between the standard deviation and the mean obtained for each of the maize parameters was applied to the mean values of the corresponding parameters of the 12 other crop types to derive their standard deviation. Regarding the soil-related parameters, the mean and standard deviation of Ze were fixed for all the 37 agricultural seasons, as well as the standard deviations of $f_{clay}$ and $f_{sand}$. Table 3 summarizes the mean and standard deviation values used to generate samples for the nine analyzed parameters.

| Parameters | Range of mean values [MIN; MAX] | References for mean values | Standard deviation values [MIN; MAX] | References for standard deviation values |
|---|---|---|---|---|

| | | | | |
|---|---|---|---|---|
| a_Fc (-) | [1.33; 1.72] | Linear relationship Fc=a_Fc·NDVI+b_Fc, built for each crop type with satellite observation (NDVI observed at bare soil and at full vegetation) | [0.09; 0.12] | Ratio between standard deviation and mean of maize (7%) applied to all crop types |
| b_Fc (-) | [-0.20; -0.36] | | [0.05; 0.09] | Ratio between standard deviation and mean of maize (25%) applied to all crop types |
| a_Kcb (-) | [1.33; 1.72] | Linear relationship Kcb=a_Kcb·NDVI+b_Kcb, built as for a_Fc and b_Fc | [0.09; 0.12] | Ratio between standard deviation and mean of maize (7%) applied to all crop types |
| b_Kcb (-) | [-0.20; -0.36] | | [0.05; 0.09] | Ratio between standard deviation and mean of maize (25%) applied to all crop types |
| Zr_max (mm) | [500; 1500] | Allen et al. (1998); Pereira et al. (2021); Rallo et al. (2021) | [125; 208] | Ratio between standard deviation and mean of maize (16%, Allen et al., 1998) applied to all crop types |
| p (-) | [0.30; 0.65] | Allen et al. (1998); Pereira et al. (2021); Rallo et al. (2021) | [0.05; 0.09] | Ratio between standard deviation and mean of maize (16%, Allen et al., 1998) applied to all |

| | | | | |
|---|---|---|---|---|
| | | | | crop types |
| $f_{clay}$ (-) | [0.24; 0.55] | Soil analysis | 0.075 | Order of magnitude of uncertainties reported in the SoilGrids product (Hengl et al., 2017) |
| $f_{sand}$ (-) | [0.10; 0.375] | | 0.075 | |
| Ze (mm) | 125 | Allen et al. (1998) | 11 | Allen et al. (1998) |

Table 3: Mean and standard deviation values used to generate samples for the nine analyzed parameters.

2.5. Outputs for Sobol indices computation: Root-Mean-Square Deviation

The Root-Mean-Square Deviation (RMSD) performance metric was used to calculate the Sobol indices. For each of the 37 agricultural seasons, 33,000 RMSD were calculated for both ET and DP, corresponding to the 33,000 parameters samples used for SAMIR simulations. The RMSD formula is written as follows:

$$RMSD = \sqrt{\frac{\sum_{i=1}^{j}(\hat{y}_i - y_i)^2}{j}} \quad (7)$$

where j is the number of days in the simulated time series, i is one day of the time series, $\hat{y}_i$ is a simulated variable time series, and $y_i$ is a reference variable time series. In this study, the reference variable time series $y_i$ were obtained for each agricultural season by averaging the 33,000 simulated time series.

2.6. Deriving a FAO-2Kc Sensitivity Proxy ($SP_{FAO\text{-}2Kc}$) from field conditions

Once the Sobol indices were obtained for the nine parameters, a correlation was sought between them and the soil-vegetation-atmosphere characteristics of the 37 agricultural seasons. The idea was to confront the Sobol indices with different criteria (soil texture, crop

type, cumulative rainfall, mean ET0, mean NDVI, modeled crop water stress level, etc.) until a satisfactory correlation was observed. From this correlation, a proxy of the sensitivity of the SAMIR parameters ($SP_{FAO\text{-}2Kc}$) has been proposed.

## 3. Results and discussion

The results of the Sobol sensitivity analysis of SAMIR are presented and discussed in this section. Sections 3.1-3.3 focus on the model sensitivity for ET simulations, while section 3.4 is about the DP simulations. First, the parameter sensitivity obtained for the 37 agricultural seasons are investigated (section 3.1). Then, a FAO-2Kc Sensitivity Proxy ($SP_{FAO\text{-}2Kc}$) is proposed to explain and predict the SAMIR's parameter sensitivity from the on-site characteristics solely (section 3.2). Next, the interactions between parameters are studied to better assess their sensitivity, and to be able to select a minimum parameter set for calibration (section 3.3). Finally, for DP, the similarities and differences with the ET case are discussed, and the main results are presented (section 3.4).

### 3.1. Parameters sensitivity for ET simulations

Each group of PHENO (a_Fc, b_Fc, a_Kcb, b_Kcb) and STRESS (Zr_max, p, $f_{clay}$, $f_{sand}$, Ze) parameters is involved in distinct and clearly identified processes as explained in section 2.1. This leads us to hypothesize that these two groups will have significant differences in terms of $STi_{norm}$ values. For each PHENO and STRESS group we summed the $STi_{norm}$ of their parameters and named these sums PHENO-$STi_{norm}$ and STRESS-$STi_{norm}$.

Table 4 reports the STi, Si, and $STi_{norm}$ values obtained for three selected agricultural seasons, which were found to reflect well the different sensitivity types. LAM_Wheat_11 is a stress-sensitive agricultural season, CAT_Maize2_21 a phenology-sensitive one, and MEX_Chilli_08 has a balanced sensitivity. A stress-sensitive (phenology-sensitive) agricultural season is characterized by a STRESS-$STi_{norm}$ (PHENO-$STi_{norm}$) greater than 66%, respectively. Similarly, a balanced agricultural season has a PHENO-$STi_{norm}$ (and a STRESS-$STi_{norm}$) between 33% and 66%. In Table 4, the first column corresponding to LAM_Wheat_11 shows a STRESS-$STi_{norm}$ equal to 81%. It means that for this agricultural season, the five STRESS parameters account for 81% of the RMSD variation and thus for

81% of the total sensitivity of the SAMIR's parameters. Among these parameters, Zr_max, p, and $f_{clay}$ showed to be the most sensitive, having higher $STi_{norm}$. Ze, which has a STi value equal to the one of the dummy parameter, ends up with a $STi_{norm}$ equal to 0. PHENO-$STi_{norm}$ of CAT_Maize2_21 is equal to 100%, indicating that it corresponds to a phenology-sensitive site. The PHENO-$STi_{norm}$ of MEX_Chilli_08 is equal to 64% reflecting a balanced sensitivity.

| Parameters | LAM_Wheat_11 | | | CAT_Maize2_21 | | | MEX_Chilli_08 | | |
|---|---|---|---|---|---|---|---|---|---|
| | STi | Si | $STi_{norm}$ | STi | Si | $STi_{norm}$ | STi | Si | $STi_{norm}$ |
| a_Fc (-) | 0,02 | 0,04 | 1% | 0,21 | 0,30 | 16% | 0,38 | -0,02 | 13% |
| b_Fc (-) | 0,02 | 0,03 | 1% | 0,10 | 0,06 | 9% | 0,51 | 0,01 | 20% |
| a_Kcb (-) | 0,13 | 0,07 | 9% | 0,73 | 0,34 | 47% | 0,39 | 0,01 | 14% |
| b_Kcb (-) | 0,13 | 0,01 | 8% | 0,41 | 0,16 | 28% | 0,44 | 0,07 | 17% |
| Zr_max (mm) | 0,44 | 0,18 | 29% | 0,05 | 0,05 | 0 | 0,33 | 0,09 | 10% |
| p (-) | 0,36 | 0,31 | 23% | 0,05 | 0,06 | 0 | 0,23 | 0,01 | 3% |
| $f_{clay}$ (-) | 0,31 | 0,02 | 20% | 0,05 | 0,05 | 0 | 0,39 | 0,01 | 13% |
| $f_{sand}$ (-) | 0,15 | 0,03 | 9% | 0,05 | 0,05 | 0 | 0,30 | 0,01 | 8% |
| Ze (mm) | 0,00 | 0,02 | 0 | 0,05 | 0,05 | 0 | 0,21 | -0,02 | 2% |
| Dummy (-) | 0,00 | 0,02 | 0 | 0,05 | 0,05 | 0 | 0,18 | -0,05 | 0 |
| PHENO group (a_Fc, b_Fc, a_Kcb, b_Kcb) | - | - | 19% | - | - | 100% | - | - | 64% |
| STRESS group (Zr_max, p, $f_{clay}$, $f_{sand}$, Ze) | - | - | 81% | - | - | 0 | - | - | 36% |

Table 4: Example of Si, STi, and $STi_{norm}$ values obtained for three contrasted agricultural seasons.

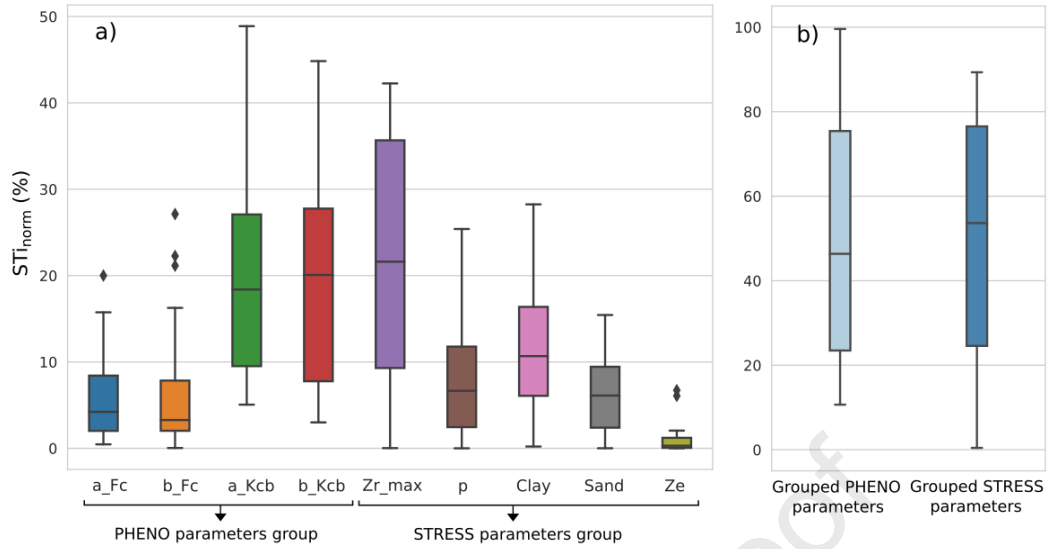


Figure 2: Boxplots of the STi$_{norm}$ of a) the nine parameters analyzed separately, and of b) the PHENO and STRESS parameter groups. Results are for ET simulations for all the 37 agricultural seasons.

Figure 2.a shows boxplots of the STi$_{norm}$ of the nine parameters analyzed separately, and Figure 2.b shows the boxplots of the STi$_{norm}$ of the parameter groups (PHENO-STi$_{norm}$ and STRESS-STi$_{norm}$), obtained for the 37 agricultural seasons. Two elements stand out in this figure: i) a_Kcb, b_Kcb, and Zr_max have in most cases a larger STi$_{norm}$ than the other parameters, with however a large dispersion (first quartile Q1 is 0.1 for a_Kcb, b_Kcb, and Zr_max, and third quartile Q3 is 0.28 for a_Kcb and b_Kcb, and 0.37 for Zr_max), ii) PHENO-STi$_{norm}$ and STRESS-STi$_{norm}$ (Figure 2.b) are nearly identical with a large dispersion for both parameter groups (Q1 and Q3 are 0.23 and 0.78 respectively). This large dispersion indicates that from one agricultural season to another, and therefore from one agro-pedo-climatic context to another, the parameter sensitivity can vary significantly.

In Figure 3, results are presented grouped by the three types of sensitivity found within the agricultural seasons: stress-sensitive, phenology-sensitive, and balanced. Figure 3.a shows that for the majority of the 12 phenology-sensitive agricultural seasons, a_Kcb and b_Kcb have the largest STi$_{norm}$. Figure 3.c shows that for the 15 stress-sensitive agricultural seasons Zr_max has the largest STi$_{norm}$ with a mean value of 36%. For these agricultural seasons, $f_{clay}$ also shows a certain level of sensitivity (mean STi$_{norm}$ is 18%). In Figure 3.e showing the 10

balanced agricultural seasons, the three parameters a_Kcb, b_Kcb, and Zr_max, already identified as the most sensitive, stand out.

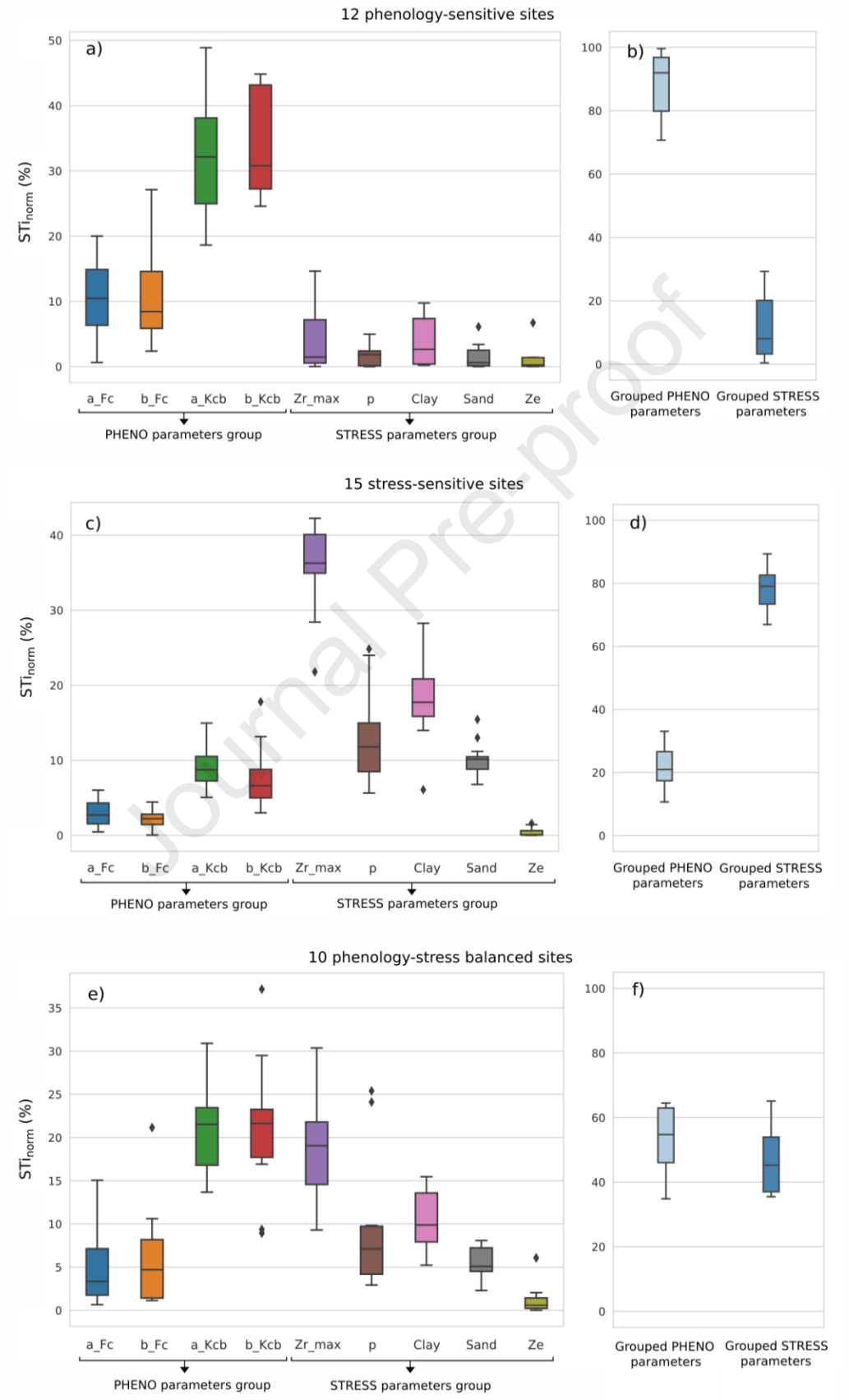

Figure 3: Boxplots of the $STi_{norm}$ of the nine analyzed parameters separately (left) and the parameters summed by PHENO and STRESS parameter group (right) for the 12 phenology-sensitive (top), the 15 stress-sensitive (middle), and the 10 balanced (bottom) agricultural seasons. These results are for ET simulations.

The fact that very contrasting or even opposite types of sensitivity were identified between the 12 phenology-sensitive and the 15 stress-sensitive agricultural seasons confirms the relevance of gathering the parameters into PHENO and STRESS groups. Figures 2 and 3 highlight distinct sensitivity types being well represented among the 37 agricultural seasons. They also indicate which parameters are the most sensitive depending on the type of agricultural season: a_Kcb and b_Kcb for the phenology-sensitive ones (dominated by the PHENO parameter group), Zr_max for the stress-sensitive ones (dominated by the STRESS group), and a_Kcb, b_Kcb, and Zr_max for the balanced ones.

### 3.2. Searching for $SP_{FAO\text{-}2Kc}$ for ET simulations

As a step further, we tried to find a proxy for SAMIR sensitivity ($SP_{FAO\text{-}2Kc}$) based on the agro-pedo-climatic characteristics of agricultural seasons. Different criteria were tested and confronted with the $STI_{norm}$ of the parameter groups (PHENO-$STi_{norm}$ and STRESS-$STI_{norm}$) for all agricultural seasons. Through trial and error, a good correlation emerged ($r^2$=0.84) between the modeled stress intensity in the root zone, calculated with an average set of parameters, and the $STi_{norm}$ of the parameter groups (Figure 4). Formally, $SP_{FAO\text{-}2Kc}$ is written as follows:

$$SP_{FAO-2Kc} = \frac{\sum_{i=1}^{d} Ks_i}{d}, \quad if \ Ks_i < 1 \ and \ \frac{Kcb_i}{Kcb_{max}} > 0.2 \tag{8}$$

with d being the number of days of the simulated time series when the crop is stressed (Ks lower than 1) and when the crop coefficient (Kcb) is larger than 20% of its maximum value, i being a specific day meeting this condition, $Ks_i$ being a daily value of Ks, and $Kcb_i$ being a daily value of Kcb. To simplify the interpretation of $SP_{FAO\text{-}2Kc}$, we normalized it between the minimum (0.41) and the maximum (0.93) of the $SP_{FAO\text{-}2Kc}$ values obtained among the 37 agricultural seasons.

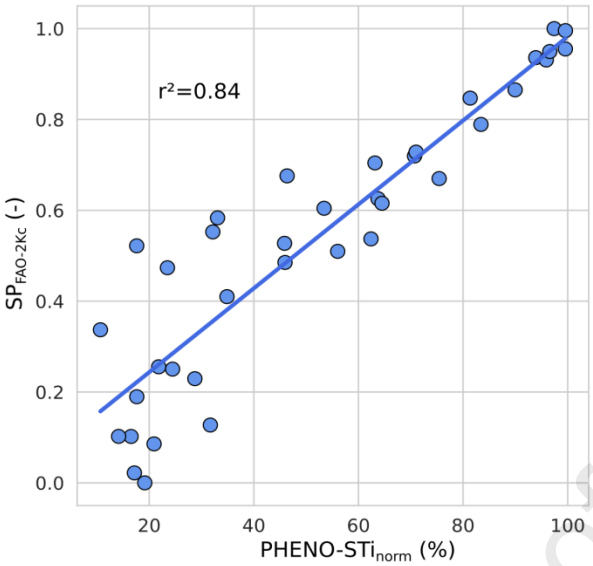


Figure 4: Correlation between $SP_{FAO\text{-}2Kc}$ and $PHENO\text{-}STi_{norm}$ for ET simulations over the 37 agricultural seasons.

$SP_{FAO\text{-}2Kc}$ can be understood as follows: the more an average set of parameters of an agricultural season generates intense crop water stress levels (related to Ks values lower than 1) at times when potential T is significant, the more the parameters belonging to the STRESS group will weigh in the model sensitivity. To figure out why this indice emerged rather than another, we must seek to better understand how SAMIR works and how the different modeled processes influence the RMSD of simulated ET. Figure 5 shows the mean time series of four SAMIR outputs for LAM_Wheat_11 and CAT_Maize2_21, and their associated uncertainties (represented with Q1 and Q3). LAM_Wheat_11 is a non-irrigated winter wheat crop, with significant precipitation in winter and spring until April/May, followed by a decrease in rainfall resulting in water stress from April. It is a stress-sensitive agricultural season ($STRESS\text{-}STi_{norm}$ is 81%). CAT_Maize2_21 is a heavily irrigated summer maize crop with no water stress (Ks=1) throughout the season. It is a phenology-sensitive agricultural season with a $PHENO\text{-}STi_{norm}$ equal to 100%.

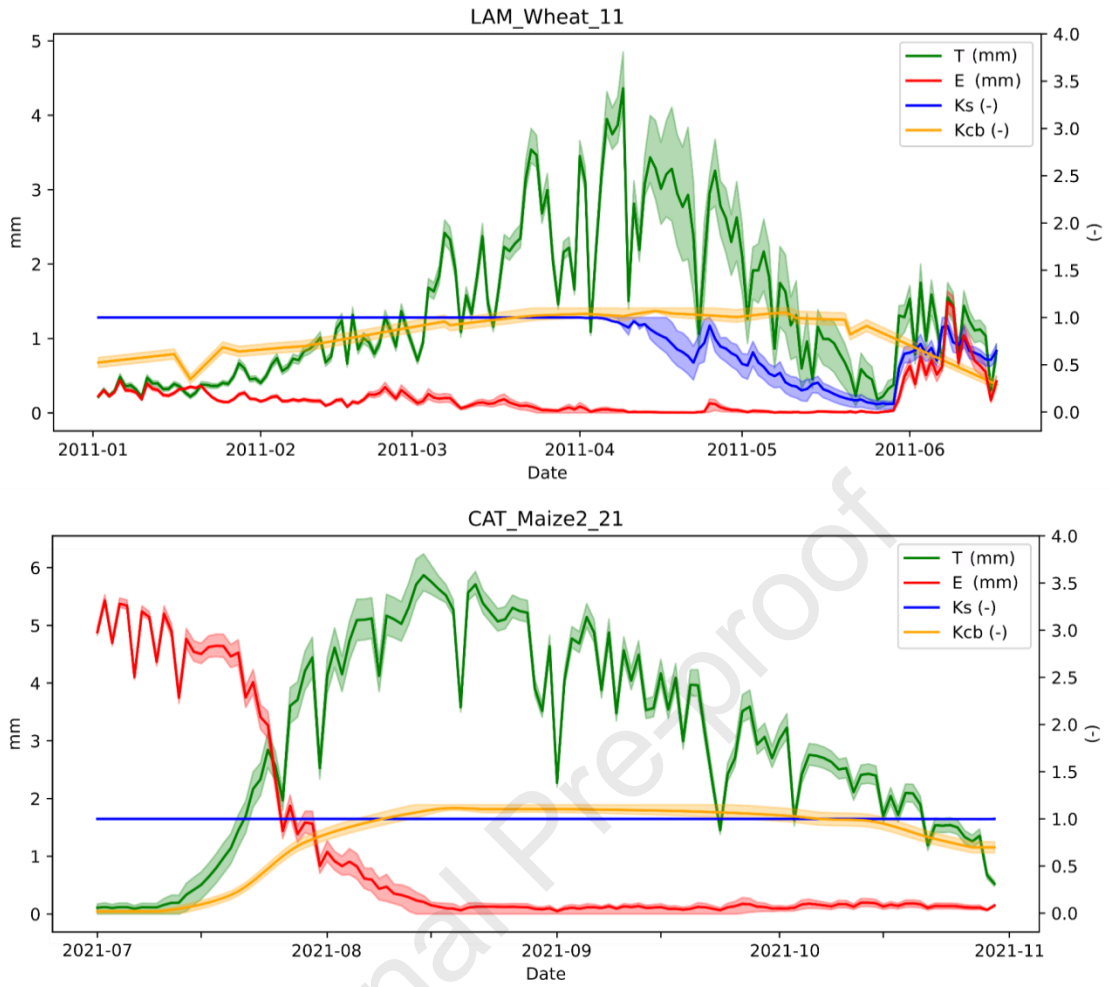


Figure 5: Daily time series of Ks, Kcb, T, and E for LAM_Wheat_11 (top) and CAT_Maize2_21 (bottom) obtained from 33,000 simulations, with their mean (lines) and uncertainties represented with Q1 and Q3 (shaded areas) respectively.

Simulated time series of LAM_Wheat_11 and CAT_Maize2_21 illustrated in Figure 5, and the $STi_{norm}$ values shown in Table 4, provide keys to understand the relevance of $SP_{FAO\text{-}2Kc}$ (equation 8):

i) In Figure 5 we see that there are more uncertainties associated with T than with E. This explains why a_Kcb, b_Kcb, and Zr_max stand out to be more sensitive (Table 4), as they are related to T process. It also explains why the parameters $f_{clay}$, $f_{sand}$, Ze, and even a_Fc and b_Fc are less sensitive, as they are partly or entirely associated with E process. Such differences in the level of uncertainties between T and E can be explained by the fact that i) the simulated time series of the 37 agricultural seasons include few bare soil periods (fraction

cover higher than 0.75 most of the time), and ii) the formalism for E simulation generates less uncertainty than the formalism related to T simulation.

ii) The uncertainties in T and E related to a_Kcb and b_Kcb are practically constant during the whole simulated period (an uncertainty associated to Kcb is always present on each simulated day) but are considerably less important than the uncertainties in T associated to water stress (i.e., when Ks is lower than 1).

iii) During the simulated periods when Ks is lower than 1, the uncertainties associated with T can be very large. If the water stress lasts long enough, while Ks is decreasing, the STRESS parameters (and thus mostly Zr_max) become more sensitive than the PHENO parameters, as is the case for LAM_Wheat_11.

iv) When there is no water stress (Ks equal to 1) as for CAT_Maize2_21, the uncertainties associated with T are entirely related to the PHENO parameters, and thus essentially to a_Kcb and b_Kcb.

The above four points help understand why $SP_{FAO\text{-}2Kc}$, based on the modeled crop water stress intensity, emerged as an efficient proxy for the model sensitivity. Indeed, when there is little water stress (Ks close to 1) the uncertainties generated by the STRESS parameters are low. This is explained by the fact that Ks is a bounded variable whose maximum value is fixed at 1, resulting in limiting the uncertainties caused by the STRESS parameters when Ks is close to 1. By contrast, when there are more intense stress episodes, the soil moisture content of the root reservoir (and thus the Ks value) takes time to decrease, generating a longer period with larger uncertainties associated with T. Consequently, the longer and more intense the stress episode is, the more T simulations will be affected by the STRESS parameters, and the more they will weigh in the final sensitivity of the agricultural season.

Note that, although the correlation between $SP_{FAO\text{-}2Kc}$ and PHENO-$STi_{norm}$ is close to 1, the relationship shows a significant variability when PHENO-$STi_{norm}$ is below 30%. This is because $SP_{FAO\text{-}2Kc}$ is less effective for agricultural seasons dominated by the stress parameters (with low PHENO-$STi_{norm}$).

### 3.3. Interactions between parameters

Figure 6 shows boxplots with the total interactions of the nine analyzed parameters for the 37 agricultural seasons for ET simulations. The total interactions of a parameter (calculated by subtracting Si to STi) reflect how this parameter indirectly affects the sensitivity of all the other parameters when its value is changed. The knowledge of the total interactions, coupled with a certain knowledge of the SAMIR model, gives enough information to select the minimum parameter set to be calibrated among the parameters being the most sensitive. The knowledge of SAMIR that is of interest here is that the PHENO and the STRESS parameter groups are involved in very different processes and have little relationship with each other.

As mentioned in section 2.3.1, for a given agricultural season, the lower the sum of its Si the higher the general level of interaction between its parameters. Here, the 37 agricultural seasons have globally important levels of interactions since the sum of their Si is on average relatively low (0.48), with a minimum of 0.17 and a maximum of 0.68. In Figure 6 we can see that among the PHENO group, a_Kcb and b_Kcb concentrate most of the total interactions. This makes sense since they are part of the same linear relationship linking Kcb to NDVI. This means that when a_Kcb is modified for calibration, it greatly affects the b_Kcb sensitivity, and conversely. Therefore, calibrating only one of these two parameters is somehow equivalent to calibrating the Kcb-NDVI relationship, in addition to avoiding compensation effects between them. Herein, we chose to calibrate a_Kcb rather than b_Kcb, because a_Kcb has a greater influence on the vegetation growth, being a time when the T demand is generally high. Regarding the STRESS group, almost all the total interactions are shared between Zr_max, $f_{clay}$ and $f_{sand}$. These three parameters interact strongly with each other as they are all involved in the size of the root reservoir, which is the key element governing the occurrence and intensity of water stress. Therefore, as with a_Kcb and b_Kcb, calibration of only one of these three parameters can be sufficient to indirectly calibrate the root reservoir. We recommend calibrating Zr_max rather than $f_{clay}$ and $f_{sand}$ because Zr_max appeared to be the most sensitive, and because no validated maximum root depth maps are currently available, as opposed to soil texture maps.

From this parameter interactions analysis, it appears that out of the nine parameters, only two, a_Kcb and Zr_max, can explain most of the model sensitivity. These parameters can be calibrated either together or individually depending on the value of $SP_{FAO\text{-}2Kc}$ and the available computer resources.

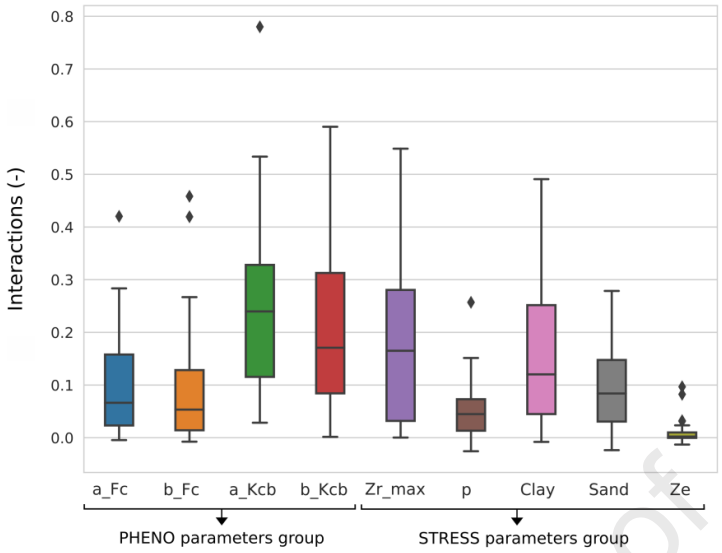


Figure 6: Boxplots of the total interactions for ET simulations of the nine analyzed parameters for the 37 agricultural seasons.

### 3.4. Parameters sensitivity for DP simulations and relationship with agricultural season characteristics

This section deals with the sensitivity of the RMSD calculated for DP simulation. It goes into less detail than for ET simulation and focuses on the similarities and differences between DP and ET cases. Herein, only 31 of the 37 agricultural seasons were analyzed because six had no DP event. As for the ET case, the parameters were gathered into STRESS and PHENO groups, and the most sensitive ones were a_Kcb, b_Kcb, Zr_max, and to a lesser extent $f_{clay}$ and $f_{sand}$ (not shown).

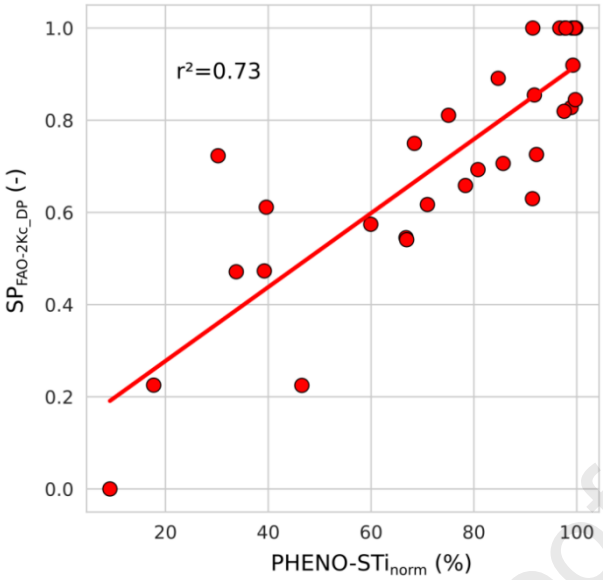


Figure 7: Correlation between $SP_{FAO\text{-}2Kc\_DP}$ and $PHENO\text{-}STi_{norm}$ for DP simulations for 31 agricultural seasons.

The sensitivity proxy for DP simulations ($SP_{FAO\text{-}2Kc\_DP}$) is similar to the one proposed for ET ($SP_{FAO\text{-}2Kc}$), with the only difference being that the period used to calculate it excludes the days following the last DP event. Indeed, the days following the last DP event, and their associated agro-climatic conditions, do not count in the generation of any DP event.

Figure 7 shows the relationship between $SP_{FAO\text{-}2Kc\_DP}$ and $PHENO\text{-}STI_{norm}$ for DP simulations. A determination coefficient of 0.73 was obtained. The lower correlation obtained for DP than for ET ($r^2$=0.84) can be explained by the higher complexity of the parameters sensitivity for DP simulations. Indeed, in SAMIR, the DP events are punctual, and each of them has its own sensitivity according to what occurred during the period just before. The final sensitivity of the parameters can thus be seen as the product of several $STi_{norm}$ obtained for each DP event. Also, especially for agricultural seasons with few DP events, the period prior to the last DP events may have involved a significant portion of bare soil, which would potentially lead to a higher sensitivity of the evaporation-related parameters. This lower correlation may also be related to the fact that the 31 agricultural seasons are less homogeneously distributed between phenology-sensitive and stress-sensitive agricultural seasons, with 21 agricultural seasons being phenology-sensitive and only four being stress-sensitive.

3.5. Overall results in brief

The Sobol sensitivity analysis for both ET and DP simulations, as well as the sensitivity proxy $SP_{FAO\text{-}2Kc}$ and the total interaction analysis, revealed several guidelines for the calibration of the FAO-2Kc-based model SAMIR:

i) for $SP_{FAO\text{-}2Kc}$ greater than 0.66 (phenology-sensitive agricultural season): a_Kcb should be selected for calibration.

ii) for $SP_{FAO\text{-}2Kc}$ lower than 0.33 (stress-sensitive agricultural season): it should be Zr_max.

iii) for $SP_{FAO\text{-}2Kc}$ between 0.33 and 0.66 (balanced agricultural season): it should be both a_Kcb and Zr_max.

Note that the above recommendations only apply in the case where the number of parameters to be calibrated should be minimized at maximum, because of computer resources limitation or equifinality issues. If there are no such issues, it is possible to calibrate both a_Kcb and Zr_max in every case. Also, by focusing either on a_Kcb or Zr_max, only certain aspects of the simulated time series would be considered in the calibration. For example, if only a_Kcb is calibrated for a phenology-sensitive agricultural season with a $SP_{FAO\text{-}2Kc}$ equal to 0.70 (thus having some water stress periods), the days when ET or DP are impacted by crop water stress would not be considered in the calibration, because a_Kcb only affects the T demand. In contrast, if only Zr_max is calibrated for a stress-sensitive agricultural season having a $SP_{FAO\text{-}2Kc}$ equal to 0.30, the focus is only given to the periods when the amount of T is reduced by water stress, neglecting the days without water stress in the calibration process.

In summary, depending notably on the computer capacities available, we recommend that the user calibrate both Zr_max and a_Kcb together, or choose between the two based on the $SP_{FAO\text{-}2Kc}$ calculated for the studied agricultural season (see Table 5).

Moreover, by choosing to calibrate only a_Kcb and/or Zr_max, and thus only T-related parameters, the days with bare soil or very little vegetation are not or poorly taken into account in the calibration. We found that under the conditions of the studied agricultural seasons the parameters related to E appear to be much less sensitive than the parameters

associated with T (as shown and explained in section 3.1). However, it is worth mentioning that the parameters related to E may be important to consider on specific agricultural seasons (not included in this study) with long and wetted bare soil periods.

| SAMIR sensitivity type | Definition | Parameter(s) to calibrate |
|---|---|---|
| Phenology-sensitive | PHENO-$STi_{norm}$ > 66% and STRESS-$STi_{norm}$ < 33% | a_Kcb (if $SP_{FAO-2Kc}$ > 0.66) |
| Stress-sensitive | STRESS-$STi_{norm}$ > 66% and PHENO-$STi_{norm}$ <33% | Zr_max (if $SP_{FAO-2Kc}$ < 0.33) |
| Balanced | 33% <= PHENO-$STi_{norm}$ <= 66% and 33% <= STRESS-$STi_{norm}$ <= 66% | a_Kcb and Zr_max (if 0.33 >= $SP_{FAO-2Kc}$ >= 0.66) |

Table 5: Three types of SAMIR sensitivity depending on the range of PHENO-$STi_{norm}$ and STRESS-$STi_{norm}$, with the recommended parameters to be calibrated according to $SP_{FAO-2Kc}$ (in case where the number of parameters to be calibrated must be optimized).

## 4. Conclusion

FAO-2Kc-based models are increasingly applied in a spatialized way to simulate the inward and outward water fluxes over extended agricultural areas (e.g., irrigation district). It requires knowing the sensitivity of the uncertain input parameters in order to be able to calibrate them spatially and optimally, and to face computational and equifinality issues. However, although these models have been widely used, no proper sensitivity analysis has yet been done.

To fill the gap, this paper investigated the sensitivity of the FAO-2Kc-based crop water balance model SAMIR for the simulation of ET and DP, considering the potential influence of different site characteristics. For this purpose, we applied the Sobol sensitivity analysis method on 10 instrumented sites and a total of 37 agricultural seasons, being diverse in terms of climate, pedology, and agricultural practices. Sobol sensitivity indices were calculated for

nine SAMIR parameters, and a correlation between them and the agricultural season's conditions was sought.

Sobol's sensitivity indices indicate that three (among the nine) parameters stand out, weighing on average 63% in the sensitivity of SAMIR ET: a_Kcb and b_Kcb related to phenology, and Zr_max related to crop water stress. It also appears that the importance of the PHENO and STRESS parameter groups in the SAMIR sensitivity varies greatly from one agricultural season to another depending on the modeled crop water stress intensity. A proxy for the sensitivity of SAMIR ($SP_{FAO\text{-}2Kc}$) has thus been proposed as the average of the crop stress coefficient (Ks) on the days when there is crop water stress (Ks lower than 1) and when the crop coefficient (Kcb) is larger than 20% of its maximum value ($Kcb > 0.2 \cdot Kcb\_max$). $SP_{FAO\text{-}2Kc}$ is able to determine 84% of the variability in SAMIR ET sensitivity (73% for the DP case) among all agricultural seasons considered.

The total interactions analysis coupled to our knowledge of the SAMIR model revealed a strong interaction between a_Kcb and b_Kcb, as well as between Zr_max, $f_{clay}$ and $f_{sand}$. This further highlights the importance of the sensitivity of a_Kcb, b_Kcb, and Zr_max, and led us to retain only a_Kcb and Zr_max for calibration. If the user has no limitation in terms of computing capacity, he can calibrate both a_Kcb and Zr_max. If he is faced with such constraints and needs to optimize the number of parameters to be calibrated, he can use $SP_{FAO\text{-}2Kc}$ value (computed from a simulation performed with an average parameter set). When $SP_{FAO\text{-}2Kc}$ is lower than 0.33, we recommend calibrating Zr_max, when it is higher than 0.66, a_Kcb, and when it is between 0.33 and 0.66, both a_Kcb and Zr_max.

These results represent a solid basis for spatializing FAO-2Kc-based models using remotely sensed data through notably the distributed calibration of their input parameters. Such a calibration strategy could rely on the soil moisture products derived from SMOS, SMAP (e.g., Ojha et al., 2019; Paolini et al., 2021), or Sentinel-1 (e.g., El Hajj et al., 2017), and on ET products derived from Landsat 8 (Senay et al., 2016) or Sentinel-2 and Sentinel-3 (e.g., Guzinski et al., 2020) ongoing missions. In addition, new satellite missions will be launched in the coming years, such as TRISHNA (Lagouarde et al., 2018) and LSTM (Koetz et al., 2018), which will provide field-scale ET estimates at an unprecedented frequency.

Software availability

SAMIR is an open-source software and is available at the following address: https://gitlab.cesbio.omp.eu/modelisation/modspa/. Documentation can be found by visiting this link. The code is implemented in Python 3 language. Contact information: vincent.rivalland@cesbio.cnes.fr.

Acknowledgements

This study was supported by the IDEWA project (ANR-19-P026-003) of the Partnership for research and innovation in the Mediterranean area (PRIMA) program and by the Horizon 2020 ACCWA project (grant agreement # 823965) in the context of Marie Sklodowska-Curie research and innovation staff exchange (RISE) program.

References

Allen, R., Pereira, L., Smith, M., 1998. Crop evapotranspiration-Guidelines for computing crop water requirements-FAO Irrigation and drainage paper 56.

Amazirh, A., Er-Raki, S., Ojha, N., Bouras, E. houssaine, Rivalland, V., Merlin, O., Chehbouni, A., 2022. Assimilation of SMAP disaggregated soil moisture and Landsat land surface temperature to improve FAO-56 estimates of ET in semi-arid regions. Agricultural Water Management 260, 107290. https://doi.org/10.1016/j.agwat.2021.107290

Amazirh, A., Merlin, O., Er-Raki, S., Bouras, E., Chehbouni, A., 2021. Implementing a new texture-based soil evaporation reduction coefficient in the FAO dual crop coefficient method. Agricultural Water Management 250, 106827. https://doi.org/10.1016/j.agwat.2021.106827

Arrouays, D., Lagacherie, P., Hartemink, A.E., 2017. Digital soil mapping across the globe. Geoderma Regional, Digital soil mapping across the globe 9, 1–4. https://doi.org/10.1016/j.geodrs.2017.03.002

Azimi, S., Dariane, A.B., Modanesi, S., Bauer-Marschallinger, B., Bindlish, R., Wagner, W., Massari, C., 2020. Assimilation of Sentinel 1 and SMAP – based satellite soil moisture retrievals into SWAT hydrological model: the impact of satellite revisit time and product spatial resolution on flood simulations in small basins. Journal of Hydrology 581, 124367. https://doi.org/10.1016/j.jhydrol.2019.124367

Baroni, G., Tarantola, S., 2014. A General Probabilistic Framework for uncertainty and global sensitivity analysis of deterministic models: A hydrological case study. Environmental Modelling & Software 51, 26–34. https://doi.org/10.1016/j.envsoft.2013.09.022

Bellvert, J., Adeline, K., Baram, S., Pierce, L., Sanden, B.L., Smart, D.R., 2018. Monitoring Crop Evapotranspiration and Crop Coefficients over an Almond and Pistachio Orchard Throughout Remote Sensing. Remote Sensing 10, 2001. https://doi.org/10.3390/rs10122001

Bellvert, J., Jofre-Ĉekalović, C., Pelechá, A., Mata, M., Nieto, H., 2020. Feasibility of Using the Two-Source Energy Balance Model (TSEB) with Sentinel-2 and Sentinel-3 Images to Analyze the Spatio-Temporal Variability of Vine Water Status in a Vineyard. Remote Sensing 12, 2299. https://doi.org/10.3390/rs12142299

Beven, K., 2006. A manifesto for the equifinality thesis. Journal of Hydrology, The model parameter estimation experiment 320, 18–36. https://doi.org/10.1016/j.jhydrol.2005.07.007

Beven, K., Freer, J., 2001. Equifinality, data assimilation, and uncertainty estimation in mechanistic modelling of complex environmental systems using the GLUE methodology. Journal of Hydrology 249, 11–29. https://doi.org/10.1016/S0022-1694(01)00421-8

Béziat, P., Ceschia, E., Dedieu, G., 2009. Carbon balance of a three crop succession over two cropland sites in South West France. Agricultural and Forest Meteorology 149, 1628–1645. https://doi.org/10.1016/j.agrformet.2009.05.004

Bretreger, D., Yeo, I.-Y., Quijano, J., Awad, J., Hancock, G., Willgoose, G., 2019. Monitoring irrigation water use over paddock scales using climate data and landsat observations. Agricultural Water Management 221, 175–191. https://doi.org/10.1016/j.agwat.2019.05.002

Brocca, L., Ciabatta, L., Massari, C., Moramarco, T., Hahn, S., Hasenauer, S., Kidd, R., Dorigo, W., Wagner, W., Levizzani, V., 2014. Soil as a natural rain gauge: Estimating global rainfall from satellite soil moisture data. Journal of Geophysical Research: Atmospheres 119, 5128–5141. https://doi.org/10.1002/2014JD021489

Campolongo, F., Saltelli, A., Cariboni, J., 2011. From screening to quantitative sensitivity analysis. A unified approach. Computer Physics Communications 182, 978–988. https://doi.org/10.1016/j.cpc.2010.12.039

Campos, I., Neale, C.M.U., Suyker, A.E., Arkebauer, T.J., Gonçalves, I.Z., 2017. Reflectance-

based crop coefficients REDUX: For operational evapotranspiration estimates in the age of high producing hybrid varieties. Agricultural Water Management 187, 140–153. https://doi.org/10.1016/j.agwat.2017.03.022

Chirouze, J., Boulet, G., Jarlan, L., Fieuzal, R., Rodriguez, J.C., Ezzahar, J., Er-Raki, S., Bigeard, G., Merlin, O., Garatuza-Payan, J., Watts, C., Chehbouni, G., 2014. Intercomparison of four remote-sensing-based energy balance methods to retrieve surface evapotranspiration and water stress of irrigated fields in semi-arid climate. Hydrology and Earth System Sciences 18, 1165–1188. https://doi.org/10.5194/hess-18-1165-2014

Constantin, J., Willaume, M., Murgue, C., Lacroix, B., Therond, O., 2015. The soil-crop models STICS and AqYield predict yield and soil water content for irrigated crops equally well with limited data. Agricultural and Forest Meteorology 206, 55–68. https://doi.org/10.1016/j.agrformet.2015.02.011

Domínguez-Niño, J., Oliver-Manera, J., Girona, J., Casadesús, J., 2019. Differential irrigation scheduling by an automated algorithm of water balance tuned by capacitance-type soil moisture sensors. Agricultural Water Management 228. https://doi.org/10.1016/j.agwat.2019.105880

Droogers, P., Immerzeel, W.W., Lorite, I.J., 2010. Estimating actual irrigation application by remotely sensed evapotranspiration observations. Agricultural Water Management 97, 1351–1359. https://doi.org/10.1016/j.agwat.2010.03.017

Efron, B., Tibshirani, R.J., 1994. An Introduction to the Bootstrap. CRC Press.

El Hajj, M., Baghdadi, N., Zribi, M., Bazzi, H., 2017. Synergic Use of Sentinel-1 and Sentinel-2 Images for Operational Soil Moisture Mapping at High Spatial Resolution over Agricultural Areas. Remote Sensing 9, 1292. https://doi.org/10.3390/rs9121292

Er-Raki, S., Chehbouni, A., Guemouria, N., Duchemin, B., Ezzahar, J., Hadria, R., 2007. Combining FAO-56 model and ground-based remote sensing to estimate water consumptions of wheat crops in a semi-arid region. Agricultural Water Management 87, 41–54. https://doi.org/10.1016/j.agwat.2006.02.004

Er-Raki, S., Chehbouni, A., Hoedjes, J., Ezzahar, J., Duchemin, B., Jacob, F., 2008. Improvement of FAO-56 method for olive orchards through sequential assimilation of thermal infrared-based estimates of ET. Agricultural Water Management 95, 309–321.

https://doi.org/10.1016/j.agwat.2007.10.013

FAO, 2021. The state of the world's land and water resources for food and agriculture. Available online: https://www.fao.org/documents/card/fr/c/cb7654en (accessed on 1 June 2022).

Foerster, S., Kaden, K., Foerster, M., Itzerott, S., 2012. Crop type mapping using spectral–temporal profiles and phenological information. Computers and Electronics in Agriculture 89, 30–40. https://doi.org/10.1016/j.compag.2012.07.015

Folberth, C., Skalský, R., Moltchanova, E., Balkovič, J., Azevedo, L.B., Obersteiner, M., van der Velde, M., 2016. Uncertainty in soil data can outweigh climate impact signals in global crop yield simulations. Nat Commun 7, 11872. https://doi.org/10.1038/ncomms11872

Garrido-Rubio, J., González-Piqueras, J., Campos, I., Osann, A., González-Gómez, L., Calera, A., 2020. Remote sensing–based soil water balance for irrigation water accounting at plot and water user association management scale. Agricultural Water Management 238, 106236. https://doi.org/10.1016/j.agwat.2020.106236

Guzinski, R., Nieto, H., Sandholt, I., Karamitilios, G., 2020. Modelling High-Resolution Actual Evapotranspiration through Sentinel-2 and Sentinel-3 Data Fusion. Remote Sensing 12, 1433. https://doi.org/10.3390/rs12091433

Han, M., Zhang, H., Chávez, J.L., Ma, L., Trout, T.J., DeJonge, K.C., 2018. Improved soil water deficit estimation through the integration of canopy temperature measurements into a soil water balance model. Irrig Sci 36, 187–201. https://doi.org/10.1007/s00271-018-0574-z

Helman, D., Bonfil, D.J., Lensky, I.M., 2019. Crop RS-Met: A biophysical evapotranspiration and root-zone soil water content model for crops based on proximal sensing and meteorological data. Agricultural Water Management 211, 210–219. https://doi.org/10.1016/j.agwat.2018.09.043

Hengl, T., Jesus, J.M. de, Heuvelink, G.B.M., Gonzalez, M.R., Kilibarda, M., Blagotić, A., Shangguan, W., Wright, M.N., Geng, X., Bauer-Marschallinger, B., Guevara, M.A., Vargas, R., MacMillan, R.A., Batjes, N.H., Leenaars, J.G.B., Ribeiro, E., Wheeler, I., Mantel, S., Kempen, B., 2017. SoilGrids250m: Global gridded soil information based on machine learning. PLOS ONE 12, e0169748. https://doi.org/10.1371/journal.pone.0169748

Hersbach, H., Bell, B., Berrisford, P., Hirahara, S., Horányi, A., Muñoz-Sabater, J., Nicolas, J., Peubey, C., Radu, R., Schepers, D., Simmons, A., Soci, C., Abdalla, S., Abellan, X., Balsamo, G., Bechtold, P., Biavati, G., Bidlot, J., Bonavita, M., De Chiara, G., Dahlgren, P., Dee, D., Diamantakis, M., Dragani, R., Flemming, J., Forbes, R., Fuentes, M., Geer, A., Haimberger, L., Healy, S., Hogan, R.J., Hólm, E., Janisková, M., Keeley, S., Laloyaux, P., Lopez, P., Lupu, C., Radnoti, G., de Rosnay, P., Rozum, I., Vamborg, F., Villaume, S., Thépaut, J.-N., 2020. The ERA5 global reanalysis. Quarterly Journal of the Royal Meteorological Society 146, 1999–2049. https://doi.org/10.1002/qj.3803

Inglada, J., Arias, M., Tardy, B., Hagolle, O., Valero, S., Morin, D., Dedieu, G., Sepulcre, G., Bontemps, S., Defourny, P., Koetz, B., 2015. Assessment of an Operational System for Crop Type Map Production Using High Temporal and Spatial Resolution Satellite Optical Imagery. Remote Sensing 7, 12356–12379. https://doi.org/10.3390/rs70912356

Kharrou, M.H., Simonneaux, V., Er-Raki, S., Le Page, M., Khabba, S., Chehbouni, A., 2021. Assessing Irrigation Water Use with Remote Sensing-Based Soil Water Balance at an Irrigation Scheme Level in a Semi-Arid Region of Morocco. Remote Sensing 13, 1133. https://doi.org/10.3390/rs13061133

Khorashadi Zadeh, F., Nossent, J., Sarrazin, F., Pianosi, F., van Griensven, A., Wagener, T., Bauwens, W., 2017. Comparison of variance-based and moment-independent global sensitivity analysis approaches by application to the SWAT model. Environmental Modelling & Software 91, 210–222. https://doi.org/10.1016/j.envsoft.2017.02.001

Koetz, B., Bastiaanssen, W., Berger, M., Defourney, P., Del Bello, U., Drusch, M., Drinkwater, M., Duca, R., Fernandez, V., Ghent, D., Guzinski, R., Hoogeveen, J., Hook, S., Lagouarde, J.-P., Lemoine, G., Manolis, I., Martimort, P., Masek, J., Massart, M., Notarnicola, C., Sobrino, J., Udelhoven, T., 2018. High Spatio- Temporal Resolution Land Surface Temperature Mission - a Copernicus Candidate Mission in Support of Agricultural Monitoring, in: IGARSS 2018 - 2018 IEEE International Geoscience and Remote Sensing Symposium. Presented at the IGARSS 2018 - 2018 IEEE International Geoscience and Remote Sensing Symposium, pp. 8160–8162. https://doi.org/10.1109/IGARSS.2018.8517433

Lagouarde, J.-P., Bhattacharya, B.K., Crébassol, P., Gamet, P., Babu, S.S., Boulet, G., Briottet, X., Buddhiraju, K.M., Cherchali, S., Dadou, I., Dedieu, G., Gouhier, M., Hagolle, O., Irvine, M., Jacob, F., Kumar, A., Kumar, K.K., Laignel, B., Mallick, K., Murthy, C.S.,

Olioso, A., Ottlé, C., Pandya, M.R., Raju, P.V., Roujean, J.-L., Sekhar, M., Shukla, M.V., Singh, S.K., Sobrino, J., Ramakrishnan, R., 2018. The Indian-French Trishna Mission: Earth Observation in the Thermal Infrared with High Spatio-Temporal Resolution, in: IGARSS 2018 - 2018 IEEE International Geoscience and Remote Sensing Symposium. Presented at the IGARSS 2018 - 2018 IEEE International Geoscience and Remote Sensing Symposium, pp. 4078–4081. https://doi.org/10.1109/IGARSS.2018.8518720

Lehmann, P., Merlin, O., Gentine, P., Or, D., 2018. Soil Texture Effects on Surface Resistance to Bare-Soil Evaporation. Geophysical Research Letters 45, 10,398-10,405. https://doi.org/10.1029/2018GL078803

Lollato, R.P., Patrignani, A., Ochsner, T.E., Edwards, J.T., 2016. Prediction of Plant Available Water at Sowing for Winter Wheat in the Southern Great Plains. Agronomy Journal 108, 745–757. https://doi.org/10.2134/agronj2015.0433

Loosvelt, L., Peters, J., Skriver, H., Lievens, H., Van Coillie, F.M.B., De Baets, B., Verhoest, N.E.C., 2012. Random Forests as a tool for estimating uncertainty at pixel-level in SAR image classification. International Journal of Applied Earth Observation and Geoinformation 19, 173–184. https://doi.org/10.1016/j.jag.2012.05.011

Massari, C., Modanesi, S., Dari, J., Gruber, A., De Lannoy, G.J.M., Girotto, M., Quintana-Seguí, P., Le Page, M., Jarlan, L., Zribi, M., Ouaadi, N., Vreugdenhil, M., Zappa, L., Dorigo, W., Wagner, W., Brombacher, J., Pelgrum, H., Jaquot, P., Freeman, V., Volden, E., Fernandez Prieto, D., Tarpanelli, A., Barbetta, S., Brocca, L., 2021. A Review of Irrigation Information Retrievals from Space and Their Utility for Users. Remote Sensing 13, 4112. https://doi.org/10.3390/rs13204112

Merlin, O., Olivera-Guerra, L., Aït Hssaine, B., Amazirh, A., Rafi, Z., Ezzahar, J., Gentine, P., Khabba, S., Gascoin, S., Er-Raki, S., 2018. A phenomenological model of soil evaporative efficiency using surface soil moisture and temperature data. Agricultural and Forest Meteorology 256–257, 501–515. https://doi.org/10.1016/j.agrformet.2018.04.010

Merlin, O., Stefan, V.G., Amazirh, A., Chanzy, A., Ceschia, E., Er-Raki, S., Gentine, P., Tallec, T., Ezzahar, J., Bircher, S., Beringer, J., Khabba, S., 2016. Modeling soil evaporation efficiency in a range of soil and atmospheric conditions using a meta-analysis approach. Water Resources Research 52, 3663–3684. https://doi.org/10.1002/2015WR018233

Neitsch, S.L., Arnold, J.G., Kiniry, J.R., Williams, J.R., 2011. Soil and Water Assessment Tool Theoretical Documentation Version 2009 (Technical Report). Texas Water Resources Institute.

Nossent, J., Elsen, P., Bauwens, W., 2011. Sobol' sensitivity analysis of a complex environmental model. Environmental Modelling & Software 26, 1515–1525. https://doi.org/10.1016/j.envsoft.2011.08.010

Ojha, N., Merlin, O., Molero, B., Suere, C., Olivera-Guerra, L., Ait Hssaine, B., Amazirh, A., Al Bitar, A., Escorihuela, M.J., Er-Raki, S., 2019. Stepwise Disaggregation of SMAP Soil Moisture at 100 m Resolution Using Landsat-7/8 Data and a Varying Intermediate Resolution. Remote Sensing 11, 1863. https://doi.org/10.3390/rs11161863

Olivera-Guerra, L., Merlin, O., Er-Raki, S., 2020. Irrigation retrieval from Landsat optical/thermal data integrated into a crop water balance model: A case study over winter wheat fields in a semi-arid region. Remote Sensing of Environment 239. https://doi.org/10.1016/j.rse.2019.111627

Olivera-Guerra, L., Merlin, O., Er-Raki, S., Khabba, S., Escorihuela, M.J., 2018. Estimating the water budget components of irrigated crops: Combining the FAO-56 dual crop coefficient with surface temperature and vegetation index data. Agricultural Water Management 208, 120–131. https://doi.org/10.1016/j.agwat.2018.06.014

Ouaadi, N., Jarlan, L., Khabba, S., Ezzahar, J., Le Page, M., Merlin, O., 2021. Irrigation Amounts and Timing Retrieval through Data Assimilation of Surface Soil Moisture into the FAO-56 Approach in the South Mediterranean Region. Remote Sensing 13, 2667. https://doi.org/10.3390/rs13142667

Paolini, G., Escorihuela, M.J., Bellvert, J., Merlin, O., 2022. Disaggregation of SMAP Soil Moisture at 20 m Resolution: Validation and Sub-Field Scale Analysis. Remote Sensing 14, 167. https://doi.org/10.3390/rs14010167

Paredes, P., Rodrigues, G.C., Alves, I., Pereira, L.S., 2014. Partitioning evapotranspiration, yield prediction and economic returns of maize under various irrigation management strategies. Agricultural Water Management 135, 27–39. https://doi.org/10.1016/j.agwat.2013.12.010

Pereira, L.S., Paredes, P., Hunsaker, D.J., López-Urrea, R., Jovanovic, N., 2021. Updates and

advances to the FAO56 crop water requirements method. Agricultural Water Management 248, 106697. https://doi.org/10.1016/j.agwat.2020.106697

Pereira, L.S., Paredes, P., Jovanovic, N., 2020. Soil water balance models for determining crop water and irrigation requirements and irrigation scheduling focusing on the FAO56 method and the dual Kc approach. Agricultural Water Management 241, 106357. https://doi.org/10.1016/j.agwat.2020.106357

Pianosi, F., Sarrazin, F., Wagener, T., 2015. A Matlab toolbox for Global Sensitivity Analysis. Environmental Modelling & Software 70. https://doi.org/10.1016/j.envsoft.2015.04.009

Poggio, L., de Sousa, L.M., Batjes, N.H., Heuvelink, G.B.M., Kempen, B., Ribeiro, E., Rossiter, D., 2021. SoilGrids 2.0: producing soil information for the globe with quantified spatial uncertainty. SOIL 7, 217–240. https://doi.org/10.5194/soil-7-217-2021

Raes, D., Steduto, P., Hsiao, T.C., Fereres, E., 2009. AquaCrop—The FAO Crop Model to Simulate Yield Response to Water: II. Main Algorithms and Software Description. Agronomy Journal 101, 438–447. https://doi.org/10.2134/agronj2008.0140s

Rafi, Z., Merlin, O., Le Dantec, V., Khabba, S., Mordelet, P., Er-Raki, S., Amazirh, A., Olivera-Guerra, L., Ait Hssaine, B., Simonneaux, V., Ezzahar, J., Ferrer, F., 2019. Partitioning evapotranspiration of a drip-irrigated wheat crop: Inter-comparing eddy covariance-, sap flow-, lysimeter- and FAO-based methods. Agricultural and Forest Meteorology 265, 310–326. https://doi.org/10.1016/j.agrformet.2018.11.031

Rallo, G., Paço, T.A., Paredes, P., Puig-Sirera, À., Massai, R., Provenzano, G., Pereira, L.S., 2021. Updated single and dual crop coefficients for tree and vine fruit crops. Agricultural Water Management 250, 106645. https://doi.org/10.1016/j.agwat.2020.106645

Román Dobarco, M., Cousin, I., Le Bas, C., Martin, M.P., 2019. Pedotransfer functions for predicting available water capacity in French soils, their applicability domain and associated uncertainty. Geoderma 336, 81–95. https://doi.org/10.1016/j.geoderma.2018.08.022

Rosa, R.D., Paredes, P., Rodrigues, G.C., Alves, I., Fernando, R.M., Pereira, L.S., Allen, R.G., 2012a. Implementing the dual crop coefficient approach in interactive software. 1. Background and computational strategy. Agricultural Water Management 103, 8–24. https://doi.org/10.1016/j.agwat.2011.10.013

Rosa, R.D., Paredes, P., Rodrigues, G.C., Fernando, R.M., Alves, I., Pereira, L.S., Allen, R.G., 2012b. Implementing the dual crop coefficient approach in interactive software: 2. Model testing. Agricultural Water Management 103, 62–77. https://doi.org/10.1016/j.agwat.2011.10.018

Saadi, S., 2018. Spatial estimation of actual evapotranspiration and irrigation volumes using water and energy balance models forced by optical remote sensing data (VIS/NIR/TIR). Université Paul Sabatier - Toulouse III ; Université de Carthage (Tunisie).

Saadi, S., Simonneaux, V., Boulet, G., Raimbault, B., Mougenot, B., Fanise, P., Ayari, H., Lili-Chabaane, Z., 2015. Monitoring Irrigation Consumption Using High Resolution NDVI Image Time Series: Calibration and Validation in the Kairouan Plain (Tunisia). Remote Sensing 7, 13005–13028. https://doi.org/10.3390/rs71013005

Saltelli, A., Annoni, P., 2010. How to avoid a perfunctory sensitivity analysis. Environmental Modelling & Software 25, 1508–1517. https://doi.org/10.1016/j.envsoft.2010.04.012

Saltelli, A., Annoni, P., Azzini, I., Campolongo, F., Ratto, M., Tarantola, S., 2010. Variance based sensitivity analysis of model output. Design and estimator for the total sensitivity index. Computer Physics Communications 181, 259–270. https://doi.org/10.1016/j.cpc.2009.09.018

Saltelli, A., Ratto, M., Andres, T., Campolongo, F., Cariboni, J., Gatelli, D., Saisana, M., Tarantola, S., 2008. Global Sensitivity Analysis: The Primer. John Wiley & Sons.

Senay, G.B., Friedrichs, M., Singh, R.K., Velpuri, N.M., 2016. Evaluating Landsat 8 evapotranspiration for water use mapping in the Colorado River Basin. Remote Sensing of Environment, Landsat 8 Science Results 185, 171–185. https://doi.org/10.1016/j.rse.2015.12.043

Sheikh, V., Visser, S., Stroosnijder, L., 2009. A simple model to predict soil moisture: Bridging Event and Continuous Hydrological (BEACH) modelling. Environmental Modelling & Software 24, 542–556. https://doi.org/10.1016/j.envsoft.2008.10.005

Simonneaux, V., Lepage, M., Helson, D., Metral, J., Thomas, S., Duchemin, B., Cherkaoui, M., Kharrou, H., Berjami, B., Chehbouni, A., 2009. Estimation spatialisée de l'évapotranspiration des cultures irriguées par télédétection : application à la gestion de l'irrigation dans la plaine du Haouz (Marrakech, Maroc). Science et changements planétaires

/ Sécheresse 20, 123–130. https://doi.org/10.1684/sec.2009.0177

Sobol′, I.M., 2001. Global sensitivity indices for nonlinear mathematical models and their Monte Carlo estimates. Mathematics and Computers in Simulation, The Second IMACS Seminar on Monte Carlo Methods 55, 271–280. https://doi.org/10.1016/S0378-4754(00)00270-6

Sobol', I.M., 1993. Sensitivity analysis for non-linear mathematical models. Mathematical Modelling and Computational Experiment 1, 407–414.

Song, X., Zhang, J., Zhan, C., Xuan, Y., Ye, M., Xu, C., 2015. Global sensitivity analysis in hydrological modeling: Review of concepts, methods, theoretical framework, and applications. Journal of Hydrology 523, 739–757. https://doi.org/10.1016/j.jhydrol.2015.02.013

Tang, Y., Reed, P., van Werkhoven, K., Wagener, T., 2007. Advancing the identification and evaluation of distributed rainfall-runoff models using global sensitivity analysis. Water Resources Research 43. https://doi.org/10.1029/2006WR005813

Vidal, J.-P., Martin, E., Franchistéguy, L., Baillon, M., Soubeyroux, J.-M., 2010. A 50-year high-resolution atmospheric reanalysis over France with the Safran system. International Journal of Climatology 30, 1627–1644. https://doi.org/10.1002/joc.2003

Wu, X., Zhou, J., Wang, H., Li, Y., Zhong, B., 2015. Evaluation of irrigation water use efficiency using remote sensing in the middle reach of the Heihe river, in the semi-arid Northwestern China. Hydrological Processes 29, 2243–2257. https://doi.org/10.1002/hyp.10365

Yang, Y., Wilson, L.T., Wang, J., 2012. Site-specific and regional on-farm rice water conservation analyzer (RiceWCA): Development and evaluation of the water balance model. Agricultural Water Management 115, 66–82. https://doi.org/10.1016/j.agwat.2012.08.010

Zaussinger, F., Dorigo, W., Gruber, A., Tarpanelli, A., Filippucci, P., Brocca, L., 2019. Estimating irrigation water use over the contiguous United States by combining satellite and reanalysis soil moisture data. Hydrology and Earth System Sciences 23, 897–923. https://doi.org/10.5194/hess-23-897-2019

Zhang, B., Liu, Y., Xu, D., Zhao, N., Lei, B., Rosa, R.D., Paredes, P., Paço, T.A., Pereira,

L.S., 2013. The dual crop coefficient approach to estimate and partitioning evapotranspiration of the winter wheat–summer maize crop sequence in North China Plain. Irrig Sci 31, 1303–1316. https://doi.org/10.1007/s00271-013-0405-1

Zhang, C., Chu, J., Fu, G., 2013. Sobol''s sensitivity analysis for a distributed hydrological model of Yichun River Basin, China. https://doi.org/10.1016/J.JHYDROL.2012.12.005

Highlights

- The sensitivity of a FAO-2Kc-based crop water balance model is analyzed.
- Evapotranspiration and deep percolation are analyzed over contrasted crop sites.
- Two parameters are found to be the most sensitive (a_Kcb and Zr_max).
- A proxy for the model's sensitivity is derived from the modeled crop water stress.
- The proxy explains 73-84% of the variability in the model output sensitivity.

**Declaration of interests**

☒ The authors declare that they have no known competing financial interests or personal relationships that could have appeared to influence the work reported in this paper.

☐ The authors declare the following financial interests/personal relationships which may be considered as potential competing interests: